Effects of finite arithmetic precision on large-scale direct numerical simulation of box turbulence by spectral method

Naoya Okamoto,^{1,*} Takashi Ishihara, Mitsuo Yokokawa, And Yukio Kaneda, And Yukio K ¹Center for General Education, Aichi Institute of Technology, Yakusa-cho, Toyota 470-0392, Japan ²Faculty of Environmental, Life, Natural Science and Technology, Okayama University, Okayama 700-8530, Japan

³ Graduate School of System Informatics, Kobe University, Kobe 657-0013, Japan ⁴Graduate School of Mathematics, Nagoya University, Nagoya 464-8602, Japan



(Received 13 August 2024; accepted 9 April 2025; published 2 June 2025)

To investigate the effects of finite arithmetic precision on large-scale direct numerical simulations (DNS) of three-dimensional turbulence using a spectral method, we performed a comparative analysis between two sets of DNS: one using single arithmetic precision (AP) and the other using double AP. Each set simulated the turbulent flows of an incompressible fluid under periodic boundary conditions at Reynolds numbers (R_{λ}) of 170 and 268, with a resolution defined by $k_{\text{max}}\eta = 4$, where k_{max} denotes the maximum wave number in the DNS and η represents the Kolmogorov length scale. Special focus was given to the temporal evolution of the maximum values of local enstrophy (Ω) and local energy dissipation rate (ϵ) , as well as the moments (Ω^p) and (ϵ^p) . The comparison shows that at $R_{\lambda} = 268$, the differences in the time-dependent maximum values between double AP and single AP DNSs are negligible for short duration (t < 1.6T), where T denotes the eddy turnover time. However, these differences become significant for longer duration (t > 1.6T). For moments with p < 4, no notable differences were observed, but significant discrepancies emerged for p > 4 and t > 1.6T. In DNSs at $R_{\lambda} = 170$, the differences in both maximum values and moments were insignificant throughout the entire simulated time range. The results in the present paper suggest that the difference becomes more significant in DNSs of turbulence at higher Reynolds numbers.

DOI: 10.1103/PhysRevFluids.10.064603

I. INTRODUCTION

In studies of turbulence, it is commonly assumed that there is a certain universality in the statistics of sufficiently small scales in turbulence at sufficiently high Reynolds numbers (Re). This universality is thought to be insensitive to the details of the flow conditions such as the initial and boundary conditions. The idea of universality is underlying the seminal work of Kolmogorov [1] and is at the heart of modern developments in turbulence theories and modeling.

Direct numerical simulation (DNS) of the Navier-Stokes (NS) equations is a powerful tool for investigating turbulence. However, once one accepts the idea of universality of turbulence and wants to understand it better by DNS, the DNS should be performed at Re as high as possible. Considering the computational constraints, achieving high Re in DNS often involves using simple boundary

*Contact author: naoya@aitech.ac.jp

†Contact author: takashi_ishihara@okayama-u.ac.jp [‡]Contact author: yokokawa@port.kobe-u.ac.jp §Contact author: kaneda@math.nagoya-u.ac.jp

conditions such as periodic boundary conditions. The turbulence studied under periodic boundary conditions is referred to as "box turbulence."

In this study, we consider box turbulence of an incompressible fluid governed by the three-dimensional Navier–Stokes equations. For DNS of box turbulence, it is convenient to use Fourier transform (FT) such as

$$\hat{\boldsymbol{u}}(\boldsymbol{k}) = \frac{1}{N^3} \sum_{\boldsymbol{x}} \boldsymbol{u}(\boldsymbol{x}) \exp(i\boldsymbol{k} \cdot \boldsymbol{x}), \tag{1}$$

where k is the wavevector, $u(x) = (u_1(x), u_2(x), u_3(x))$ denotes the fluid velocity at position $x = (x, y, z) = (x_1, x_2, x_3)$, and x, y, and z are Cartesian coordinates. The velocity is assumed to be periodic in the x, y, and z directions. The symbol \sum_x denotes summation over $L \times M \times N$ grid points in the fundamental periodic box in physical space x, where L, M, and N represent the number of grid points in the x, y, and z directions, respectively. For simplicity, we assume the fundamental periodic box is a regular cube, and L = M = N.

In DNS of turbulence of an incompressible fluid, it is important to accurately operate ∇^{-2} , which is necessary for solving the pressure field. Here ∇^{-2} is the inverse Laplace operator. The so-called Fourier spectral method, which uses the FT such as in Eq. (1), has the advantage that it enables one to perform the operation efficiently and accurately, although it is limited by machine accuracy.

In DNS of high-Re turbulence using Fourier spectral method, we need to take into account of the following inequalities (i), (ii), and (iii):

- (i) $k_e \ll k_\eta$, where k_e denotes the representative wave number of the wave vector modes in the energy containing range, and k_η represents that of the energy dissipation range where most of the energy dissipates.
 - (ii) $V(k_n) \ll V(k_e)$, where V(k) indicates the representative magnitude of $\hat{\boldsymbol{u}}(\boldsymbol{k})$ at $|\boldsymbol{k}| = k$.
- (iii) $T \gg \tau_{\eta}$, where T denotes the characteristic time of energy containing eddies at $|\mathbf{k}| \sim k_e$, and τ_{η} represents the one at $|\mathbf{k}| \sim k_{\eta}$.

These facts imply the following for the DNS:

- (D-i) The cube of the number N, denoted as N^3 , must be sufficiently large to encompass at least the wave-number range k such that $k_e < k < k_\eta$.
- (D-ii) The ratio $\gamma(k) \equiv V(k)/V(k_e)$ becomes very small when k approaches k_{max} , where k_{max} represents the maximum wave number retained in the DNS.
- (D-iii) The simulation time, denoted as T_S , should not be significantly smaller than $T(\gg \tau_{\eta})$ to ensure that the DNS is minimally affected by the time-dependence of the energy-containing eddies, the statistics of which are not universally consistent with Kolmogorov's 1941 theory (K41).

With the progress of parallel computing, the feasibility of performing large-scale DNS to study high-Reynolds-number turbulence has improved. For instance, Yeung *et al.* [2,3] performed DNS with $N^3 = 32768^3 \approx 3.5 \times 10^{13}$, which, to our knowledge, is the largest in DNSs so far executed globally. In these simulations, the ratio $E(k)/E(k_e)$ at $k \approx k_{\text{max}} \approx 10^4 k_e$ is approximately 10^{-10} , where E(k) represents the energy spectrum. Given that $E(k) \propto k^2 |\hat{u}(k)|^2$ at large wave numbers, this suggests that the ratio $\gamma(k)$ defined in (D-ii) is approximately $(10^{-10})^{1/2}/10^4 = 10^{-9}$ at $k \sim k_{\text{max}}$.

It is to be recalled here that in any DNS, the arithmetic precision (AP) must be finite, so that strictly speaking any DNS may be affected by the round-off errors due to the finiteness of the AP. Provided that the AP is not so poor in a certain appropriate sense and the number N^3 is not so large, it looks reasonable to assume the effects of the finite AP on the statistics obtained by the DNS are not much larger than those of the other errors, such as those of finite resolutions in space and time as studied by Yeung *et al.* [4]. However, in view of (D-i) and (D-ii), one may wonder if it remains true when N^3 is huge, e.g., as large as 10^{13} or larger, and the ratio $\gamma(k)$ at k near k_{max} is very small, e.g., as small as 10^{-9} or less.

To clarify this issue, let us consider the sums such as

$$\hat{C}_{j}(\mathbf{k}) = i \sum_{\mathbf{q}} \hat{u}_{\alpha}(\mathbf{k} - \mathbf{q}) q_{\alpha} \hat{u}_{j}(\mathbf{q}), \tag{2}$$

which are derived from the FT of the convection term $C(x) \equiv (u \cdot \nabla)u$ in the NS equation. Here, \sum_q indicates the summation over N^3 grid points in the wave vector space $\mathbf{q} = (q_1, q_2, q_3)$, employing the summation convention for repeated Greek indices but not for italic indices. In DNS based on FT, such sums must be computed at each grid point in the wave vector space $\mathbf{k} = (k_1, k_2, k_3)$ and at every time step.

The sum in Eq. (2) can be computed efficiently through the following steps:

(C-i) First, compute u(x) and $\nabla u(x)$ using an inverse FT, such that

$$u(x) = \sum_{k} \hat{u}(k) \exp(-ik \cdot x), \tag{3}$$

(C-ii) Compute $(\mathbf{u} \cdot \nabla)\mathbf{u}$ in physical space, and then

(C-iii) Apply the FT to $(\mathbf{u} \cdot \nabla)\mathbf{u}$.

Note that steps (C-i) and (C-iii) as well as Eq. (2) involve summations over the N^3 grid points in the wave vector or physical space. In practice, to efficiently eliminate aliasing errors, one may employ a method known as phase shifting; however, this still requires summations similar to Eq. (2).

Assume that at a specific time step, the exact value of $\hat{u}(k)$ is known for any k and is represented or approximated by $\hat{u}^{\infty}(k)$ and $\hat{u}^{p}(k)$ in DNSs with infinitely accurate AP and a specified finite AP, respectively.

The relationship can be expressed as follows:

$$\hat{u}_i^p(\mathbf{k}) = \hat{u}_i^\infty(\mathbf{k}) + \hat{u}_i^\infty(\mathbf{k})\hat{\epsilon}_i(\mathbf{k}),\tag{4}$$

where $\hat{u}_i^{\infty}(\mathbf{k})\hat{\epsilon}_i(\mathbf{k})$ represents the round-off error and typically depends on AP. For example, if one uses single-AP, $|\hat{\epsilon}_i(\mathbf{k})|$ is typically of the order 10^{-8} .

Let $u^p(x)$ denotes the value of u(x) obtained by substituting $\hat{u}^p(k)$ into $\hat{u}(k)$ in Eq. (3), and performing the inverse FT with the given AP, and let $\hat{C}^p(k)$ denote the estimate of $\hat{C}(k)$ obtained by repeating (C-i) to (C-iii) with replacing u(x) by $u^p(x)$. Then, similar to Eq. (4), we may write

$$\hat{C}_i^p(\mathbf{k}) = \hat{C}_i^{\infty}(\mathbf{k}) + \hat{C}_i^{\infty}(\mathbf{k})\Delta_i^C(\mathbf{k}), \tag{5}$$

where $\hat{C}_i^{\infty}(k)$ represents the value obtained using infinitely accurate AP.

Considering first the implication of (D-i), namely, the largeness of N, note that the summations in Eqs. (1), (2), and (3) span N^3 grid points. If N^3 is large, the cumulative effect of finite AP on each summed term, although individually small, may become significant. Therefore, one may question whether $\Delta_i^C(\mathbf{k})$ can be safely ignored when N^3 reaches as high as 10^{13} , even if the round-off errors $\hat{\epsilon}_i(\mathbf{k})$ are minute, as is the case in DNSs using single AP.

Consider next the implications of (D-ii), namely, the smallness of $\gamma(k)$. If $\gamma(k)$ at very large k is exceedingly small, then the error $|\hat{u}_i^\infty(k)\hat{e}_i(k)|$ at $k \sim k_e$ is not necessarily much smaller than $|\hat{u}^\infty(k)|$ at extremely large k even if $|\hat{e}_i(k)|$ is very small. This gives rise the concern that the contributions to $u^p(x)$ computed by using FT such as (3) and the true " $\hat{u}(k)$ " at large k may be masked or contaminated by noise or errors induced by $\hat{u}_i^\infty(k)\hat{e}_i(k)$ at $k \sim k_e$. One may then ask if the errors $\Delta_i^C(k)$ remain insignificant for large $k \sim k_{\max}$. For instance, suppose that $\gamma(k)$ at a large $k \sim k_{\max}$ is as small as 10^{-9} or less, and $\hat{e}_i(k)$ can be as small as 10^{-8} . One may then wonder whether $\Delta_i^C(k)$ is still negligible at large k, for example, at $k \sim k_{\max}$.

The main objective of this study is to get some idea on the effects of the finite AP in DNS of high Re turbulence. To this end, we compared DNS statistics obtained using single AP, referred to as DNS_{SP}, with those derived from DNS using double AP, referred to as DNS_{DP}.

The comparison is made from the viewpoints of the questions noted above. In this regard, this study differs from previous studies on the effects of AP in Fourier spectral method, including the one by Homann *et al.* [5] who examined the impact of the floating-point precision on the results of DNS of turbulence by eliminating digits in pseudospectral DNS computations at 256^3 grid resolutions systematically, and the one by Wang and Rosa [6] who examined the effects of pile up of rounding-off errors in very long DNS (over 50 to 100 eddy turnover times). The grid points (N^3) and Re in our

DNS are significantly higher than those in the aforementioned studies. The present study differs also from the study by Yeung *et al.* [4] in the sense that in view of (D-iii) we continued the simulation time $T_S(>T)$ substantially longer than that of their study, where T is the eddy turnover time. Yeung *et al.* [4] showed that the statistics of DNS with single AP are not much different from those of DNS with double AP over a short time range $0 < t < 10\tau_{\eta}$, where τ_{η} is the Kolmogorov timescale. However, as seen below, DNSs over a long-time range suggest that they may be sensitive to the AP at a later stage.

To assess the effects of AP, this study focuses on the statistics of the local energy dissipation rate $\epsilon(x, t)$ and local enstrophy $\Omega(x, t)$, consistent with high-Reynolds-number turbulence DNS studies [4,7–14]. These quantities are defined as follows:

$$\Omega(\mathbf{x},t) \equiv \frac{1}{2}\omega_{\alpha}(\mathbf{x},t)\omega_{\alpha}(\mathbf{x},t),\tag{6}$$

$$\epsilon(\mathbf{x}, t) \equiv 2\nu S_{\alpha\beta}(\mathbf{x}, t) S_{\alpha\beta}(\mathbf{x}, t),$$
 (7)

where ω_{α} represents the α th component of the vorticity field, and $S_{\alpha\beta} = (\partial_{\beta}u_{\alpha} + \partial_{\alpha}u_{\beta})/2$, with ν denoting the kinematic viscosity.

The structure of this paper is as follows: Section II describes the numerical methods and simulation settings. Section III presents a comparison of DNS results computed in both double and single precision, discussing quantitively the effects of arithmetic precision across two cases of Reynolds numbers. Section IV presents conclusions and discussion.

II. NUMERICAL METHODS AND SIMULATION SETTINGS

In this study, we utilized data from the DNS of forced box turbulence in an incompressible fluid governed by the NS equation. The numerical methods employed in these DNSs are the same as those used in prior studies [15–17]. The computational domain was a cubic box with each side of 2π in the x, y, and z directions. Aliasing errors were eliminated using a phase-shift method and spherically symmetric truncation, with the maximum wave number retained in the DNSs being $k_{\text{max}} = (\sqrt{2}/3)N$. The time integration was performed using a fourth-order Runge–Kutta method. The total kinetic energy E within the box was maintained at approximately 0.5 by applying a forcing mechanism (via negative viscosity) in the low wave-number range. For additional details on the DNS method, see Refs. [15–17].

Systematic investigations by Yeung et~al.~[4] show that extreme events, evaluated by the spatial peak values of the local energy dissipation rate or local enstrophy, are well preserved in DNS with spatial and temporal resolutions satisfying $k_{\rm max}\eta \gtrsim 3$ and the Courant-Friedrichs-Lewy (CFL) number defined by $C = (|u| + |v| + |w|)_{\rm max} \Delta t/\Delta x \lesssim 0.3$ over the time range $0 < t < 10\tau_{\eta}$, where the subscript "max" indicates the maximum value across all N^3 grid points, and $\Delta x = 2\pi/N$ represents the grid spacing. Their DNSs were performed using a spectral method by Rogallo [18] combined with a second-order Runge-Kutta method to reduce aliasing errors. In this study, which uses a fully alias-free spectral method with a fourth-order Runge-Kutta method, the spatial resolution was determined as $k_{\rm max}\eta \approx 4$ and the time increment Δt was determined such that the C was approximately 0.55 or 0.275.

We performed two types of DNS, DNS_{SP} and DNS_{DP}, which respectively use single AP and double AP, for each of the four runs named RunL-C1, RunL-C2, RunH-C1, and RunH-C2. The labels "L" and "H" denote lower Reynolds number ($R_{\lambda} = 170$) and higher Reynolds number ($R_{\lambda} = 268$), respectively, whereas "C1" and "C2" indicate runs with C of 0.55 and 0.275, respectively. The main run conditions and representative turbulence characteristics are summarized in Table I. The DNS results discussed in the subsequent section are from the runs with C = 0.275, unless otherwise stated. Regarding the influence of C, readers may refer to the Appendix.

The run conditions including the initial conditions used in DNS_{SP} were identical to those in DNS_{DP} for each of the four runs. All computations were integrated up to approximately 2.5T, where T indicates the initial eddy turnover time given by T = L/u', $u' = (2E/3)^{1/2}$, and L is defined by

Run	N	R_{λ}	$10^4 \nu$	$10^4 \Delta t$	С	$k_{\rm max}$	$k_{\mathrm{max}}\eta$	T	$\langle \Omega \rangle$
RunL-C1	1024	170	7	6.25	0.55	483	3.9	2.1	58.6
RunL-C2	1024	170	7	3.125	0.275	483	3.9	2.1	58.6
RunH-C1	2048	268	2.8	3.125	0.55	965	3.9	1.9	143.6
RunH-C2	2048	268	2.8	1.5625	0.275	965	3.9	1.9	143.6

TABLE I. DNS parameters. The values of R_{λ} , η , T, and $\langle \Omega \rangle$ are those at time t = 0.

 $L = \pi/(2u'^2) \int_0^{k_{\text{max}}} E(k)/kdk$, where E(k) represents the energy spectrum and is approximated here by $E(k) = \sum_{k-1/2 \le |\boldsymbol{p}| < k+1/2} |\hat{\boldsymbol{u}}(\boldsymbol{p})|^2/2$. The Kolmogorov length scale, η , Taylor microscale length scale, λ , and R_{λ} , are respectively defined as $\eta = (\nu^3/\langle \epsilon \rangle)^{1/4}$, $\lambda = (15\nu u'^2/\langle \epsilon \rangle)^{1/2}$, and $R_{\lambda} = u'\lambda/\nu$, where $\langle \cdot \rangle$ denotes spatial average of \cdot . In the box turbulence, $\langle \epsilon \rangle = 2\nu\langle \Omega \rangle$.

We used a developed turbulent field at $R_{\lambda} = 268$, $k_{\text{max}} \eta \approx 2$, $N^3 = 1024^3$ (Dev-F) computed in Ref. [17] for setting the initial field for RunH-C1 and RunH-C2 at higher resolutions $k_{\text{max}} \eta \approx 4$. The Fourier coefficients of the initial fields of RunH-C1 and RunH-C2 are obtained by the zero padding method using those of Dev-F. Before executing RunL-C1 and RunL-C2, we performed DNS at $N^3 = 1024^3$ using Dev-F as the initial field, and continued the DNS until R_{λ} becomes quasi-stationary and approximately 170. We used the DNS field thus obtained as the initial fields for RunL-C1 and RunL-C2.

Statistics such as the moments of Ω and ϵ are computed using the double AP in both DNS_{DP} and DNS_{SP}. The visualization of the distribution of these quantities on a plane at high Reynolds numbers (Re) reveals spatially localized spiky structures (see Ref. [19]), referred to as extreme events. The spatial maxima of these structures are often several orders of magnitude greater than their spatial means. The structures of such extreme events in high-Re turbulence are generally sensitive to the accuracy of DNS, making them good indicators for evaluating the numerical accuracy of DNS for fine-scales in high-Re turbulence. They also form a key factor in the study of intermittency at small scales in high-Re turbulence. Therefore, these quantities are carefully evaluated.

III. NUMERICAL RESULTS

A. Maximum and high-order moments

Figure 1 shows the time dependence of $\epsilon_{\rm max}/\langle\epsilon\rangle_{t=0}$ and $\Omega_{\rm max}/\langle\Omega\rangle_{t=0}$ in RunH-C2 ($R_{\lambda}\approx 268$) by DNS_{DP} and DNS_{SP} as functions of t/T, where T denotes the eddy turnover time that characterizes the timescale of the energy-containing eddies. As shown in Fig. 1(a), the two curves of $\epsilon_{\rm max}/\langle\epsilon\rangle_{t=0}$ for DNS_{SP} and DNS_{DP} overlap well up to $t/T\approx 1.6$. However, the agreement between the two curves deteriorates at later time, specifically for t/T>1.6. After $t/T\sim 2.4$, there are several instances where $\epsilon_{\rm max}/\langle\epsilon\rangle_{t=0}$ in DNS_{SP} is smaller by a factor of 2 or more than that in DNS_{DP}. This suggests that DNS_{SP} may underestimate $\epsilon_{\rm max}$ and $\Omega_{\rm max}$ compared with DNS_{DP}.

A similar result is also true for the curves of $\Omega_{\rm max}/\langle\Omega\rangle_{t=0}$ shown in Fig. 1(b). The two curves overlap well in an early time range, say, $t<1.6T\sim52\tau_{\eta}$, but not later (i.e., t>1.6T), where τ_{η} is the Kolmogorov timescale defined by $t_{\eta}=(\nu/\epsilon)^{1/2}$. This overlap at the early time range is consistent with studies by Yeung *et al.* [4,8], based on DNSs at $k_{\rm max}\eta\approx2.8$, where it was shown that $\Omega_{\rm max}$ of DNS_{SP} was not significantly different from that of DNS_{DP}. However, the DNSs are only up to $t/\tau_{\eta}<12$. Figure 1 shows that even if the difference between the statistics of DNS_{SP} and DNS_{DP} is negligible in a certain initial time range, it may not be negligible in later time ranges.

In each of Figs. 1(a) and 1(b), the change of the degree of the agreement between the two curves by DNS_{SP} and DNS_{DP} appears suddenly. Such a sudden change reminds us of studies on chaotic systems, such as the Lorenz model [20]. These studies show that nonlinear systems may, in general, have a chaotic nature, for example the so-called butterfly effect, and may exhibit strong sensitivity

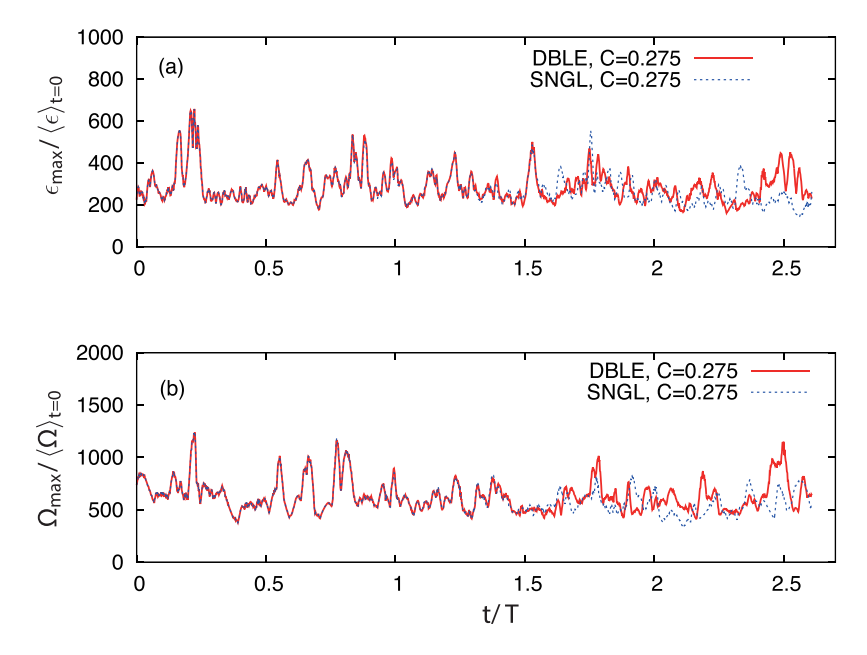


FIG. 1. (a) Local energy dissipation and (b) local enstrophy vs the normalized time t/T by DNS_{SP} and DNS_{DP} of RunH-C2 ($R_{\lambda} = 268$). They are normalized by their respective mean values at the initial instant. The tags "DBLE" and "SNGL" denote the runs by DNS_{DP} and DNS_{SP}, respectively.

to small differences in run conditions. In view of the fact that turbulence is also a strongly nonlinear phenomenon, such a sudden change may be not surprising. However, it should be noted that the number of modes in our DNS is on the order $N^3 \sim 10^9$ or more. This is much larger than those of systems commonly used in studies of chaotic systems with a small degree of freedom, such as the Lorentz model.

Figure 2 shows the pth root of the pth-order moments of ϵ and Ω (i.e., $\langle \epsilon^p \rangle^{1/p}$ and $\langle \Omega^p \rangle^{1/p}$) for RunH-C2. (Since the p-dependence of the moments is too strong, especially for large p, we take the pth root of each moment so that all the lines can be plotted on the same graph.) For clarity, a magnified version of Fig. 2 is shown in Fig. 3 for p=1,2, and 3. As observed in Fig. 1, in an early time range (t/T < 1.6), the curves of $\langle \epsilon^p \rangle^{1/p}/\langle \epsilon \rangle_{t=0}$ by DNS_{SP} overlap well with those of DNS_{DP} for $p=1,2,\cdots 7$. Later, at (t/T>1.6), a different pattern emerges. For smaller p values, such as p=1,2,3, the difference between $\langle \epsilon^p \rangle^{1/p}/\langle \epsilon \rangle_{t=0}$ using DNS_{SP} and DNS_{DP} appears to be sufficiently small. However, as p increases, this difference becomes more pronounced. A similar trend is also observed for $\langle \Omega^p \rangle^{1/p}$.

In Figs 1 and 2, it is seen that the curves by DNS_{SP} and DNS_{DP} cross each other several times in the interval 1.6 < t/T < 2.6. One might therefore wonder if there is any systematic and significant difference in the statistics by DNS_{SP} and DNS_{DP}. To see this point more clearly, we consider here the time-averages of the statistics. Let M[X] and $\sigma[X]$ be respectively the time average of X and the standard deviation given by $\sigma[X] \equiv \sqrt{M[X^2] - (M[X])^2}$. Table II lists the time averaged pth-order moments of normalized energy dissipation $\bar{\epsilon}$ and enstrophy $\bar{\Omega}$ as well as the time average of the max values of $\bar{\epsilon}$ and $\bar{\Omega}$, where $\bar{\epsilon} = \epsilon/\langle \epsilon \rangle_{t=0}$ and $\bar{\Omega} = \Omega/\langle \Omega \rangle_{t=0}$, and the time average was taken using the data of $\bar{\epsilon}$ and $\bar{\Omega}$ at about 800 time steps $t = t_n (n = 1, 2, 3, \cdots)$ spaced equally in the time interval 1.3 < t/T < 2.6.

It is seen in Table II that (i) for $p \ge 5$ there are clear differences between the statistics by DNS_{SP} and those by DNS_{DP}, although the differences are small for p < 4, (ii) as compared to DNS_{DP}, DNS_{SP} underestimates both of the means and the standard deviations of $\bar{\epsilon}$ and $\bar{\Omega}$ for $p \ge 5$, (iii) the differences between DNS_{SP} and DNS_{DP} are larger for larger p, and (iv) the differences

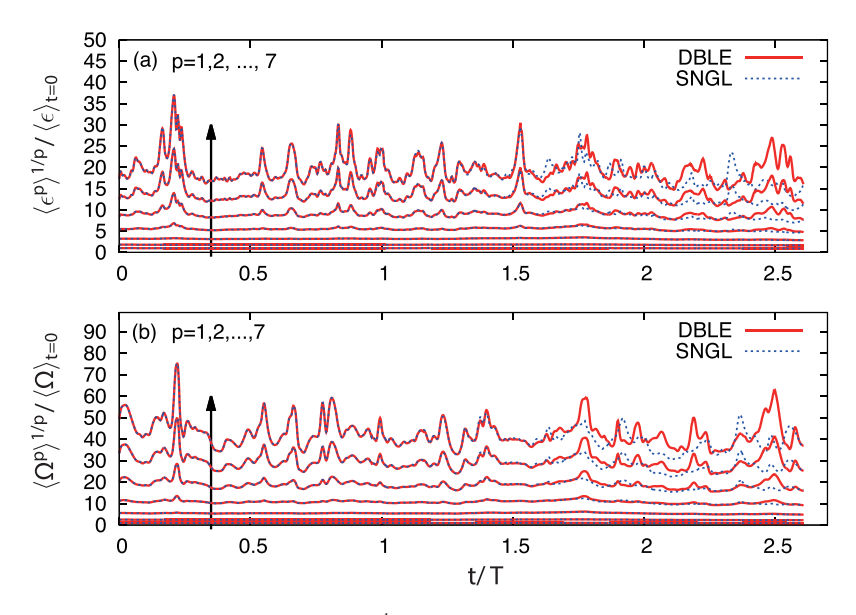


FIG. 2. (a) pth roots of the moments $\langle \epsilon^p(\mathbf{x},t) \rangle^{\frac{1}{p}} / \langle \epsilon \rangle_{t=0}$ vs t/T by DNS_{SP} and DNS_{DP} of RunH-C2. (b) The same as panel (a) but for $\langle \Omega^p(\mathbf{x},t) \rangle^{\frac{1}{p}} / \langle \Omega \rangle_{t=0}$. Arrows indicate increasing values of p.

are larger for enstrophy than for energy dissipation. Regarding (ii), consider for example, the statistics of $\bar{\Omega}^p$ for p=7. The ratios of $M[\langle \bar{\Omega}^7 \rangle]$ and $\sigma[\langle \bar{\Omega}^7 \rangle]$ by DNS_{SP} to those by DNS_{DP} are respectively $2.11/3.67 \approx 0.57$ and $1.87/5.44 \approx 0.34$, i.e., they differ by the factor of $1/0.57 \approx 1.75$ and $1/0.34 \approx 2.94$, respectively.

DNS is in general not error-free. Strictly speaking, it may be affected not only by round-off errors, but also by many other effects such as those of finite resolution in space and time, sampling numbers,

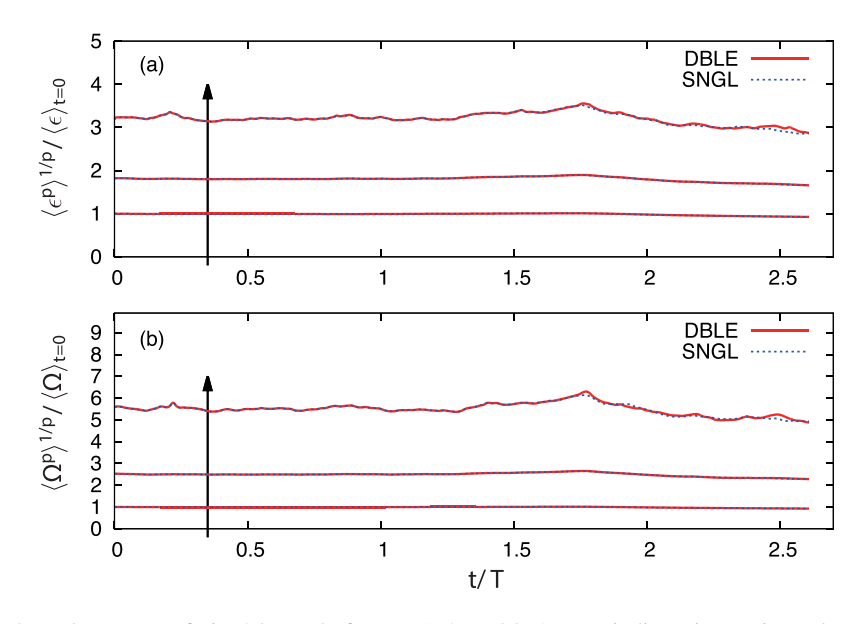


FIG. 3. Enlargement of Fig. 2 but only for p = 1, 2, and 3. Arrows indicate increasing values of p.

TABLE II. Time-averaged pth-order moments of the normalized energy dissipation $\bar{\epsilon}$ and enstrophy $\bar{\Omega}$, as well as the time averages of $\bar{\epsilon}_{max}$ and $\bar{\Omega}_{max}$, where $\bar{\epsilon} = \epsilon/\langle \epsilon \rangle_{t=0}$, $\bar{\Omega} = \Omega/\langle \Omega \rangle_{t=0}$. Here, $\bar{\epsilon}_{max}$ and $\bar{\Omega}_{max}$ represent the spatial maximum values of $\bar{\epsilon}$ and $\bar{\Omega}$. The corresponding standard deviations are also shown.

p	DBLE $(M[\langle \bar{\epsilon}^p \rangle], \sigma[\langle \bar{\epsilon}^p \rangle])$	SNGL $(M[\langle \bar{\epsilon}^p \rangle], \sigma[\langle \bar{\epsilon}^p \rangle])$	DBLE $(M[\langle \bar{\Omega}^p \rangle], \sigma[\langle \bar{\Omega}^p \rangle])$	SNGL $(M[\langle \bar{\Omega}^p \rangle], \sigma[\langle \bar{\Omega}^p \rangle])$
2	(3.22, 0.27)	(3.21, 0.27)	(6.14, 0.58)	(6.13, 0.58)
3	(33.3, 5.69)	(32.8, 5.9)	(167, 34)	(166, 33)
4	(981, 278)	(920, 290)	$(1.40, 0.48) \times 10^4$	$(1.33, 0.43) \times 10^4$
5	$(6.84, 3.44) \times 10^4$	$(5.79, 3.04) \times 10^4$	$(2.63, 1.54) \times 10^6$	$(2.21, 1.02) \times 10^6$
6	$(8.73, 7.89) \times 10^6$	$(6.54, 6.15) \times 10^6$	$(8.32, 8.21) \times 10^8$	$(5.89, 3.80) \times 10^8$
7	$(1.64, 2.42) \times 10^9$	$(1.12, 1.89) \times 10^9$	$(3.67, 5.44) \times 10^{11}$	$(2.11, 1.87) \times 10^{11}$
	$(M[\bar{\epsilon}_{\text{max}}], \sigma[\bar{\epsilon}_{\text{max}}])$ (275, 62.2)	$(M[\bar{\epsilon}_{\text{max}}], \sigma[\bar{\epsilon}_{\text{max}}])$ (256, 61.5)	$(M[\bar{\Omega}_{\text{max}}], \sigma[\bar{\Omega}_{\text{max}}])$ (611, 134)	$(M[\bar{\Omega}_{\text{max}}], \sigma[\bar{\Omega}_{\text{max}}])$ (565, 105)

etc. It may therefore be of interest to compare the magnitudes of the effects of the round-off errors discussed above with those of the other (if not all) effects.

Regarding the comparison with the effects of the space resolution, our previous DNSs [21] of box turbulence give some idea. The DNSs use the same numerical methods and forcing scheme as in the present study, and the Reynolds number is 217, which is a little smaller than 268 in the present study. Table III shows the time-averaged *p*th-order moments $M[\langle \bar{\Omega}^p \rangle]$ as well as the maximum $M[\bar{\Omega}_{max}]$ by the DNSs. It is seen that the effects of the spatial resolution are not that large. For example, even for p=7, the ratio of $M[\langle \bar{\Omega}^p \rangle]$ of the DNS with $k_{max} \eta \approx 6$ to that of the DNS with $k_{max} \eta \approx 3$ is 2.76/3.04 ≈ 0.91 . Such a week resolution dependence of the *p*th-order moments for $k_{max} \gtrsim 3$ is consistent with previous work [7]. However, it is seen in Table II that for the same p(=7), the ratio of $M[\langle \bar{\Omega}^p \rangle]$ of DNS_{SP} to that of DNS_{DP} is 2.11/3.67 ≈ 0.57 , which is considerably smaller than 0.91. This implies that the effect of the round-off error on $M[\langle \bar{\Omega}^7 \rangle]$ is more significant than that of space resolution in the present case.

Regarding the comparison with sampling effects, Table II gives some idea. For example, it is seen in Table II that the difference between $M[\langle \bar{\Omega}^7 \rangle]$ s by DNS_{DP} and DNS_{SP} is $(3.67-2.11) \times 10^{11} = 1.56 \times 10^{11}$. This difference is comparable to $\sigma[\langle \bar{\Omega}^7 \rangle] = 1.87 \times 10^{11}$ by DNS_{SP}. Since standard deviation σ is a representative measure of sampling error, this comparison suggests that the magnitudes of the effects of round-off error can be comparable to those of temporal sampling.

TABLE III. Time-averaged *p*th-order moments of the normalized enstrophy $\bar{\Omega}$ as well as the time average of its maximum values for (left) DNS at resolution $k_{\max} \eta \approx 6$ and (right) DNS at $k_{\max} \eta \approx 3$, where $\bar{\Omega} = \Omega/\langle \Omega \rangle_{t=0}$. The averaging is performed for t > 1.3T using approximately 800 fields from DNS data in Ref. [21]. The corresponding standard deviations are also shown.

p	DBLE, $k_{\text{max}} \eta \approx 6 \ (M[\langle \bar{\Omega}^p \rangle], \sigma[\langle \bar{\Omega}^p \rangle])$	DBLE $k_{\max} \eta \approx 3 \ (M[\langle \bar{\Omega}^p \rangle], \sigma[\langle \bar{\Omega}^p \rangle])$
2	(5.26, 0.193)	(5.26, 0.193)
3	(111, 8.33)	(111, 8.67)
4	$(6.11, 1.34) \times 10^3$	$(6.22, 1.41) \times 10^3$
5	$(6.65, 3.49) \times 10^5$	$(6.96, 3.55) \times 10^5$
6	$(1.15, 1.13) \times 10^8$	$(1.25, 1.12) \times 10^8$
7	$(2.76, 4.19) \times 10^{10}$	$(3.04, 4.02) \times 10^{10}$
	$(M[\bar{\Omega}_{ ext{max}}], \sigma[\bar{\Omega}_{ ext{max}}]) \ (339, 75.1)$	$(M[\bar{\Omega}_{\text{max}}], \sigma[\bar{\Omega}_{\text{max}}])$ (341, 74.1)

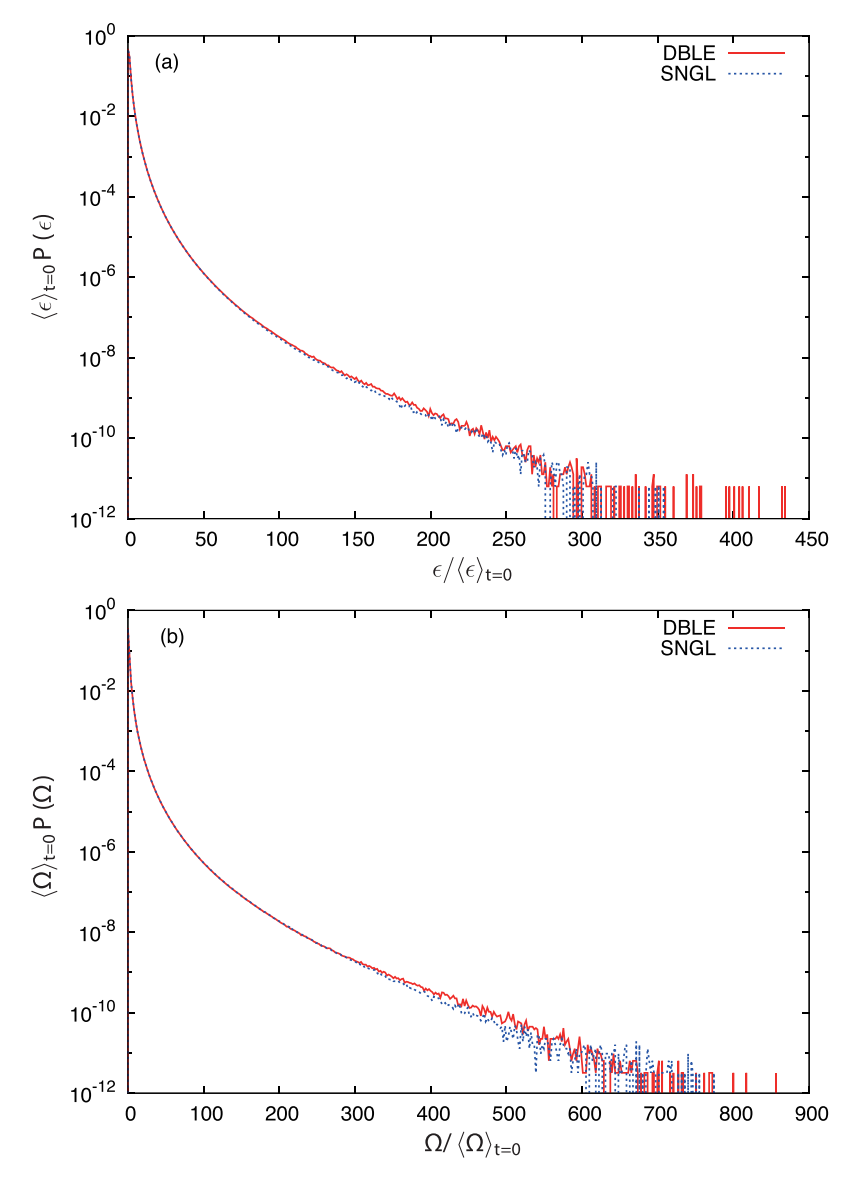


FIG. 4. PDFs of ϵ and Ω in RunH-C2.

B. PDFs of local enstrophy and dissipation

Figure 4 shows the probability density functions (PDFs) P of ϵ and Ω for RunH-C2. Since the tails of the PDFs of ϵ and Ω are fluctuating in time, we plot PDFs of ϵ and Ω averaged over a time range. Each PDF curve in Fig. 4 is obtained using the data of 17 snapshot-fields in the time range 1.3 < t/T < 2.6. The PDF of $\epsilon/\langle \epsilon \rangle_{t=0}$ by DNS_{SP} overlaps well with that of DNS_{DP} up to $\epsilon/\langle \epsilon \rangle_{t=0} \sim 120$; however, the PDF of DNS_{SP} appears smaller than that of DNS_{DP} for $150 < \epsilon/\langle \epsilon \rangle_{t=0} < 200$ and for $350 < \epsilon/\langle \epsilon \rangle_{t=0}$.

Qualitatively the same is true for the PDFs of Ω . A close inspection suggests the following: the PDF of Ω by DNS_{SP} is smaller than that by DNS_{DP} in the range $350 < \Omega/\langle \Omega \rangle_{t=0} < 600$, and the difference is larger than that for the PDF of the energy dissipation.

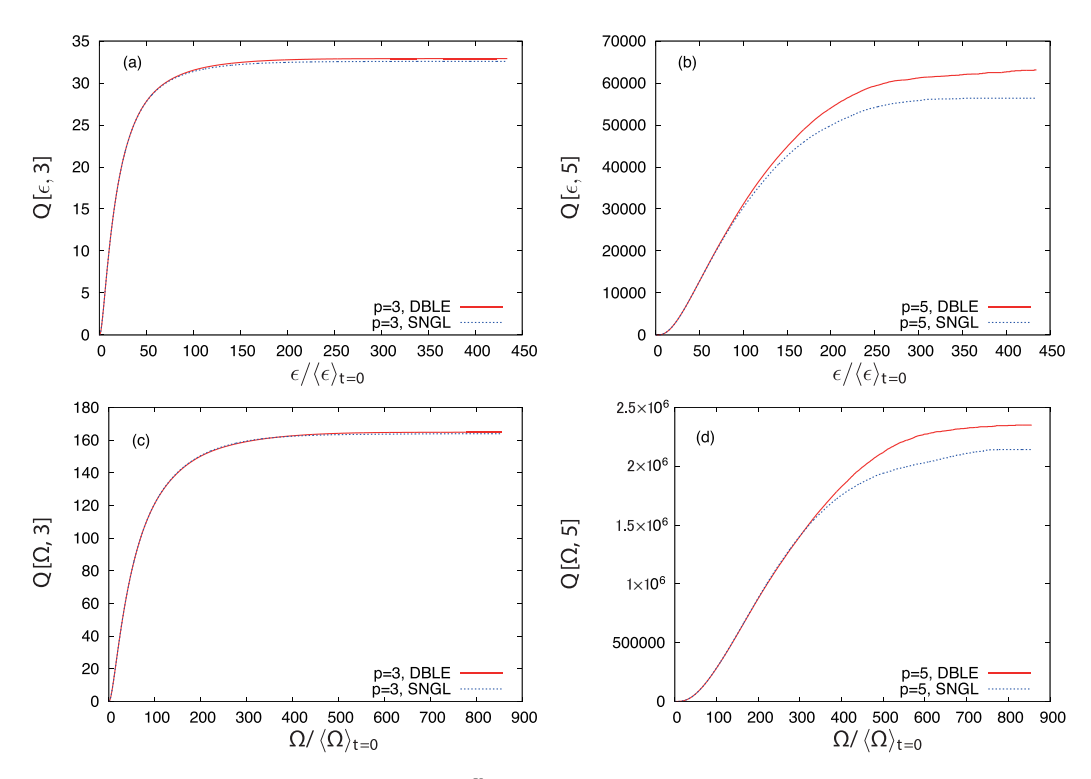


FIG. 5. Normalized integrals $Q[X, p] = \int_0^X x^p P(x) dx / \alpha^p$ vs X/α , where (X, α) is either $(\epsilon, \langle \epsilon \rangle_{t=0})$ or $(\Omega, \langle \Omega \rangle_{t=0})$ and P is the PDF corresponding to ϵ or Ω . (a) $X = \epsilon, p = 3$, (b) $X = \epsilon, p = 5$, (c) $X = \Omega, p = 3$, (d) $X = \Omega, p = 5$.

Figure 5 shows the normalized integrals $Q[X, p] = \int_0^X x^p P(x) dx/\alpha^p$, where p = 3 or 5, and (X, α) is either $(\epsilon, \langle \epsilon \rangle_{t=0})$ or $(\Omega, \langle \Omega \rangle_{t=0})$. The symbol P denotes the PDF corresponding to ϵ or Ω . The integrals Q were computed by taking the time-average of P(x) of the 17 snapshot fields used for producing Fig. 4. In the limit of $X \to \infty$, Q[X, p] yields the mean $M[\langle \bar{X}^p \rangle]$, where $\bar{X} = X/\alpha$. It is seen in Figs. 5(b) and 5(d) that DNS_{SP} (blue lines) underestimates the normalized integrals Q for p = 5 as compared to DNS_{DP} (red lines), while it is seen in Figs. 5(a) and 5(c) that the differences are small. This is consistent with the observations (i) and (ii) in Table II. Thus, in addition to Table II, Figs. 5(b) and 5(d) provide another demonstration of the systematic difference between the statistics by DNS_{SP} and DNS_{DP}.

Note: A closer inspection shows that the means $M[\langle \bar{X}^p \rangle]$ shown in Table II differ slightly from those estimated using the normalized integrals Q at large X in Fig. 5. However, it was confirmed that the means agree well with those estimated from the normalized integrals Q when calculated using the 17 snapshot fields used to produce Fig. 5. Therefore, the differences can be regarded as due to the difference between the field sets used for taking the time averages; one consists of 17 fields, while the other consists of about 800 fields.

These results suggest that sufficiently high AP is necessary for accurate computation of the tails of the PDFs of the energy dissipation and enstrophy in high Re turbulence, and one needs to be careful in using single AP in DNS of turbulence at high Re. This finding would be useful for studying extreme events represented by the far tails of the PDFs of enstrophy and energy dissipation in high-Reynolds-number turbulence [8,14].

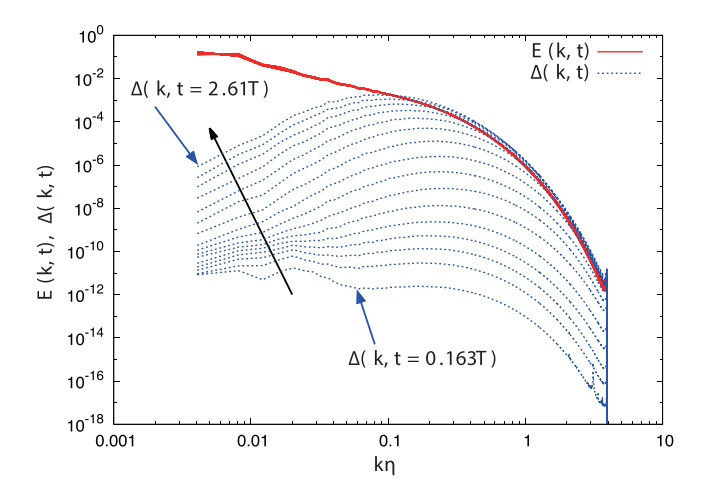


FIG. 6. Energy spectra E(k, t) and difference spectra $\Delta(k, t)$ in RunH-C2. The spectrum is represented in every $2000\Delta t$, which corresponds to 0.163T. The black arrow indicates increasing values of t/T.

C. Difference spectra

To obtain the scale-by-scale information, we consider the differences between the velocity field by DNS_{SP}, $u_{SP}(x,t)$, and that by DNS_{DP}, $u_{DP}(x,t)$. Let $\delta u(x,t) \equiv u_{DP}(x,t) - u_{SP}(x,t)$, and let $\Delta(k,t)$ be the difference spectrum defined as

$$\Delta(k,t) = \sum_{k-1/2 \leqslant k' < k+1/2} |\delta \boldsymbol{u}(k',t)|^2.$$

Figure 6 presents $\Delta(k, t)$ alongside $E(k, t) \approx E_{DP}(k, t) \approx E_{SP}(k, t)$ in RunH-C2 as a function of $k\eta$ at various time steps, where $E_{DP}(k, t)$ and $E_{SP}(k, t)$ are the energy spectra from $\mathbf{u}_{DP}(\mathbf{x}, t)$ and $\mathbf{u}_{SP}(\mathbf{x}, t)$, respectively.

The error spectrum $\Delta(k,t)$ increases over time, while $E_{\rm DP}(k,t)$ and $E_{\rm SP}(k,t)$ remain relatively constant. The error $\Delta(k,t)$ relative to E(k,t) escalates more rapidly at higher k values, indicating that the relative contamination of the field arising from round-off error increases faster in the higher-wave-number range. A detailed analysis shows that in the early time range (0.16T < t < 0.49T), there is a wave-number range $(k\eta < 0.3)$ where the k-dependence of $\Delta(k,t)$ is weak.

D. Visualization

The relative contributions to the statistics of $\epsilon^p(\Omega^p)$ from the regions of high $\epsilon(\Omega)$ as compared to those from low $\epsilon(\Omega)$ are in general larger for larger p, and the statistics for very large p are dominated by the former contributions. This and the results presented in Sec. II A, in particular Table II, suggest that the differences between the statistics by DNS_{SP} and DNS_{DP} are more prominent in high $\epsilon(\Omega)$ -regions than the low $\epsilon(\Omega)$ -regions.

To get some insight into how the effects of round-off errors appear in the physical space, we plot in Fig. 7 intense enstrophy regions at a time instant; Fig. 7 shows the 512³ subcube which contains the point of the highest enstrophy in DNS_{DP}. Figures 7(a) and 7(b), respectively, show the intense enstrophy regions in RunH-C2 by DNS_{DP} and DNS_{SP}, while Fig. 7(c) is the superposition of Figs. 7(a) and 7(b). Comparing Figs. 7(a) and 7(b) shows that the DNS_{SP} and DNS_{DP} fields are similar to each other in the sense of coarse graining; both fields show similar clusters of tubelike structures. However, Fig. 7(c) shows that the two fields do not exactly coincide. For example, a long vortex structure and a clumped structure, marked by red and green arrows, respectively, are observed in Fig. 7(b), while they are either absent or less visible in Fig. 7(a). Thus, Fig. 7 shows that

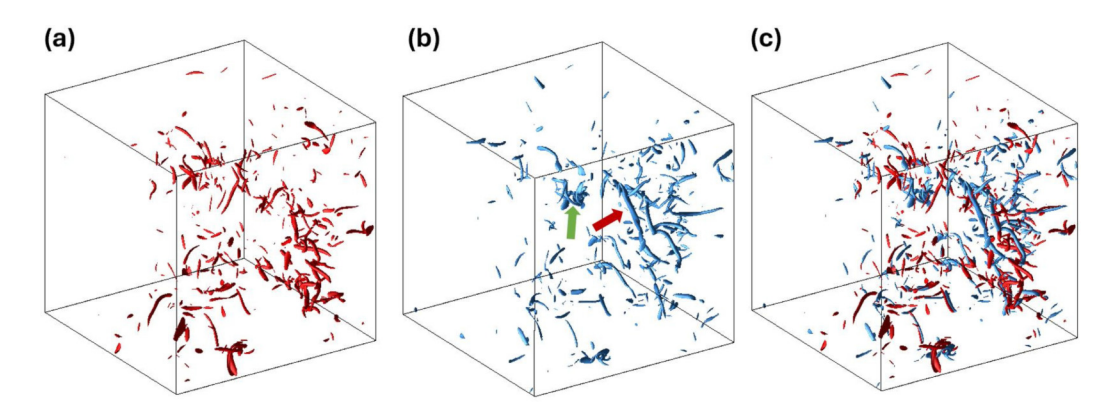


FIG. 7. Intense vorticity regions of the flow field by (a) DNS_{DP}, (b) DNS_{SP} of RunH-C2 at t/T = 2.45, and (c) superposition of panels (a) and (b). The isosurfaces of vorticity are displayed in $|\omega| = M_{DP} + 6.5\sigma_{DP}$, where M_{DP} and σ_{DP} denote the mean value and standard deviation of the modulus of the vorticity field DNS_{DP} of RunH-C2. Only the 512³ subcubes among 2048³ grid points are displayed for the ease of comparison. Red and green arrows respectively mark a long vortex structure and a clumped structure.

the intense enstrophy regions by DNS_{SP} may differ from those by DNS_{DP} in their relative positions and structures(shapes) at small scales, but the differences are not so prominent at large scales. This is consistent with the results discussed in Sec. II C, in the sense that the (relative) differences between DNS_{SP} and DNS_{DP} are more prominent at small scales than at large scales.

E. Revnolds number dependence

To investigate the possible dependence of statistical sensitivity on Re with respect to AP, we performed an additional simulation (RunL-C2) at a lower Reynolds number ($R_{\lambda} = x170$), compared to RunH-C2 ($R_{\lambda} = 268$). Figures 8–12 present the statistics for RunL-C2, with comparative data from RunH-C2.

Figures 8 and 9 show both low- and high-order statistics, including local dissipation rate and local enstrophy, by DNS_{SP} and DNS_{DP}. For lower-order statistics ($\langle \epsilon^p \rangle$, $\langle \Omega^p \rangle$ for p=1,2,3), the differences between DNS_{SP} and DNS_{DP} are negligible throughout the time range examined (0 < t < 2.6T), regardless of whether the Reynolds number is lower or higher.

However, for higher-order statistics ($\langle \epsilon^p \rangle$, $\langle \Omega^p \rangle$ for p > 4) and spatial maxima ($\epsilon_{\rm max}$, $\Omega_{\rm max}$), notable differences in sensitivity to AP emerge between RunH-C2 and RunL-C2. In RunH-C2, statistics from DNS_{SP} differ significantly from those obtained with DNS_{DP} in the time range (t > 1.6T), whereas in RunL-C2, such differences are nearly imperceptible throughout the entire time range (0 < t < 2.4T).

These findings indicate that lower-order statistics are robust against AP or rounding-off errors across different Reynolds numbers. In contrast, higher-order statistics, which are sensitive to the nature of extreme events, demonstrate increased sensitivity at higher Reynolds numbers. This sensitivity underscores the significance of accounting for rounding-off errors when analyzing extreme events in high-Re turbulence.

Figure 10 illustrates the PDFs of the local dissipation rate and local enstrophy. In RunL-C2, the PDFs from DNS_{DP} and DNS_{SP} exhibit minor differences, whereas in RunH-C2, the PDF tails from DNS_{SP} are noticeably underestimated compared to those from DNS_{DP} .

This underestimation aligns with findings from a previous study [5]. Since the tails of the PDFs significantly influence higher-order statistics, the results in Fig. 10 is consistent with those observed in Figs 8 and 9. These PDF results further emphasize the necessity of meticulous consideration of rounding-off errors when studying extreme events in high-Reynolds-number turbulence.

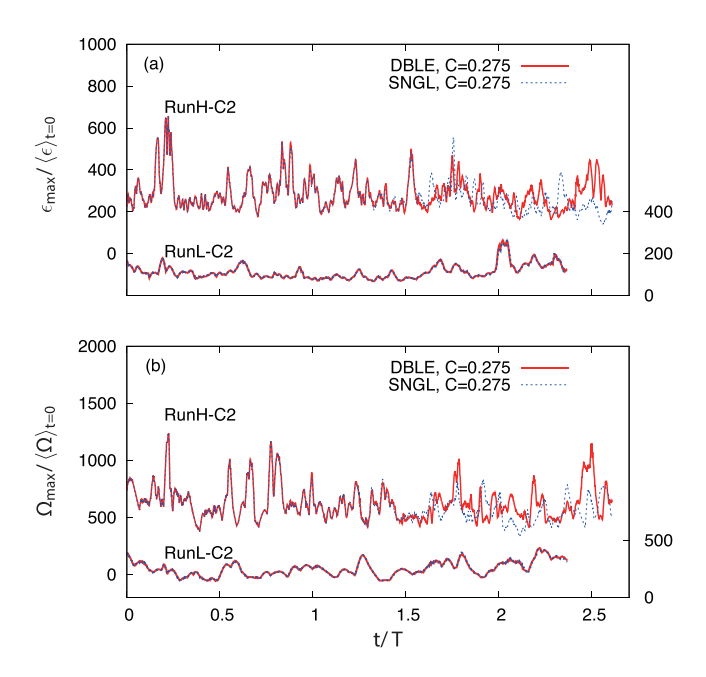


FIG. 8. Time dependence of the maximum value of (a) local dissipation and (b) local enstrophy. Scales on the left and right are for RunH-C2 ($R_{\lambda} = 268$) and RunL-C2 ($R_{\lambda} = 170$), respectively.

Figure 11 illustrates the regions of intense vorticity in RunH-C2 and RunL-C2 at later times. For clarity, only a $1/(4^3)$ subregion of the entire computational domain is displayed. In RunH-C2, a noticeable difference in the location of the vorticity structures is observed between the DNS_{DP} and DNS_{SP} simulations, whereas in RunL-C2, this difference is nearly imperceptible. Therefore, the intense vorticity structures are more sensitive to the AP at higher Re.

Figure 12 presents the energy and difference spectra at various times for RunH-C2 and RunL-C2. The difference spectra increase more rapidly at higher Reynolds numbers when time is normalized by the eddy turnover time *T*.

IV. CONCLUSIONS AND DISCUSSION

To investigate the effects of finite arithmetic precision on large-scale DNS of three-dimensional turbulence using the spectral method, we have compared the statistics of two sets of DNSs of turbulent flows in a periodic box. One of the sets consists of DNSs at $R_{\lambda} = 170$ and 268 with double AP, and the other consists of those with single AP. The comparison of the turbulence statistics shows the following:

- (1) At $R_{\lambda}=268$, the time dependence of the pth-order moments of ϵ and Ω , as well as the spatial maximum values of ϵ and Ω , i.e., $\epsilon_{\rm max}$ and $\Omega_{\rm max}$, by the DNS with single AP (DNS_{SP}) agree well with those by the DNS with double AP DNS_{DP} at t<1.6T. But the agreement is poor for t>1.6T. Compared to DNS_{DP}, DNS_{SP} underestimates the time averages (over the time 1.3T < t < 2.6T) of the pth-order moments, $\epsilon_{\rm max}$ and $\Omega_{\rm max}$, and also their standard deviations. The differences between the statistics by DNS_{DP} and DNS_{SP} are larger for the enstrophy than energy dissipation, and for larger p.
- (2) At $R_{\lambda} = 170$, the differences between the statistics by DNS_{SP} and DNS_{DP} are small for the entire simulated time domain.

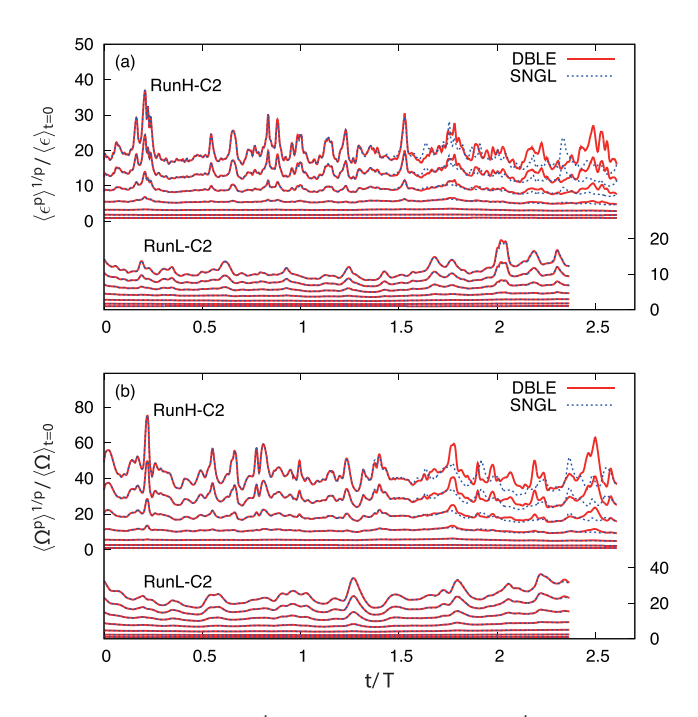


FIG. 9. Time dependence of (a) $\langle \epsilon^p(\mathbf{x},t) \rangle^{\frac{1}{p}}/\langle \epsilon \rangle_{t=0}$ and (b) $\langle \Omega^p(\mathbf{x},t) \rangle^{\frac{1}{p}}/\langle \Omega \rangle_{t=0}$ for $p=1,2,\cdots,7$. Scales on the left and right are for RunH-C2 and RunL-C2, respectively.

These results suggest that some statistics under certain conditions, such as the time-averages of the high-order moments of ϵ or Ω under the conditions used in this study, i.e., at $R_{\lambda} \approx 268$, $N \approx 2000$, and $T_s/T \approx 2.6$, may be sensitive to the difference of AP.

It would then be natural to ask, "What are the guidelines for determining when DP or precision higher than SP is necessary?" A naive consideration suggests that the required AP would be larger for larger R_{λ} , $k_{\text{max}}\eta$, N, and T_s , and also that one need be careful in using single AP for studying statistics dominated by modes (eddies) whose amplitudes are smaller than by a factor of 10^{-8} or less as compared with those of energy containing modes (eddies), because SP computations may not properly treat fields with magnitudes spanning over 8 orders or so.

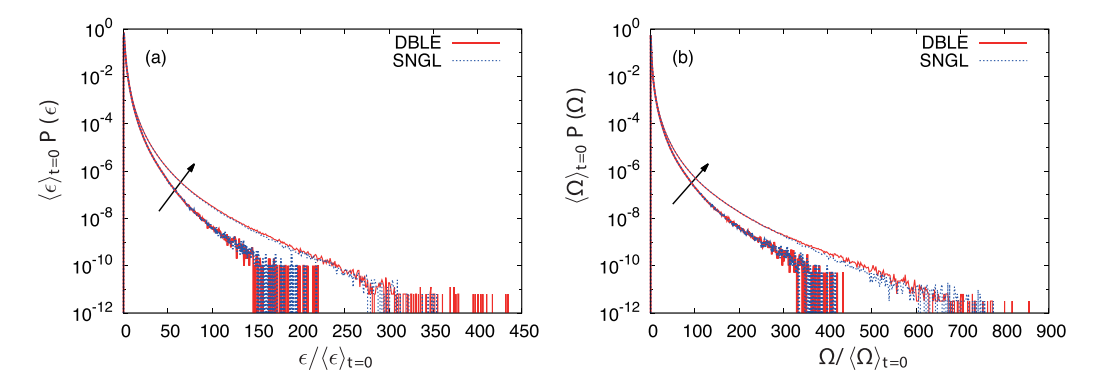


FIG. 10. (a) $\langle \epsilon \rangle_{t=0} P[\epsilon]$ vs $\epsilon/\langle \epsilon \rangle_{t=0}$ in RunH-C2 and RunL-C2. (b) $\langle \Omega \rangle_{t=0} P[\Omega]$ vs $\Omega/\langle \Omega \rangle_{t=0}$ in RunH-C2 and RunL-C2. The arrows indicate increasing values of R_{λ} .

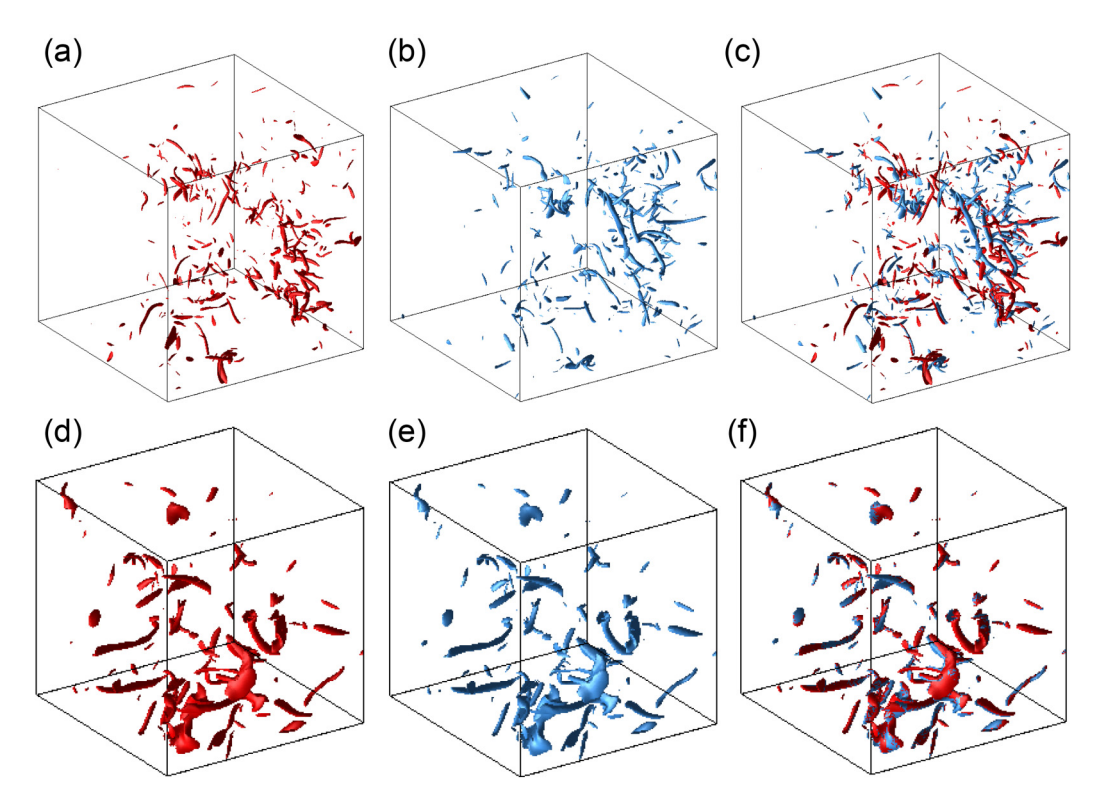


FIG. 11. Intense vorticity regions of the flow field by (a) DNS_{DP}, (b) DNS_{SP} of RunH-C2 at t/T = 2.45, and (c) superposition of panels (a) and (b). (d), (e), and (f) is similar to panels (a), (b), and (c), respectively, but in RunL-C2 at t/T = 2.37. The isosurfaces of vorticity are plotted for $|\omega| = M_{DP} + 6.5\sigma_{DP}$, where M_{DP} and σ_{DP} respectively denote the mean value and standard deviation of the modulus of the vorticity field by DNS_{DP} of RunH-C2 (for the top row) or RunL-C2 (for the bottom row).

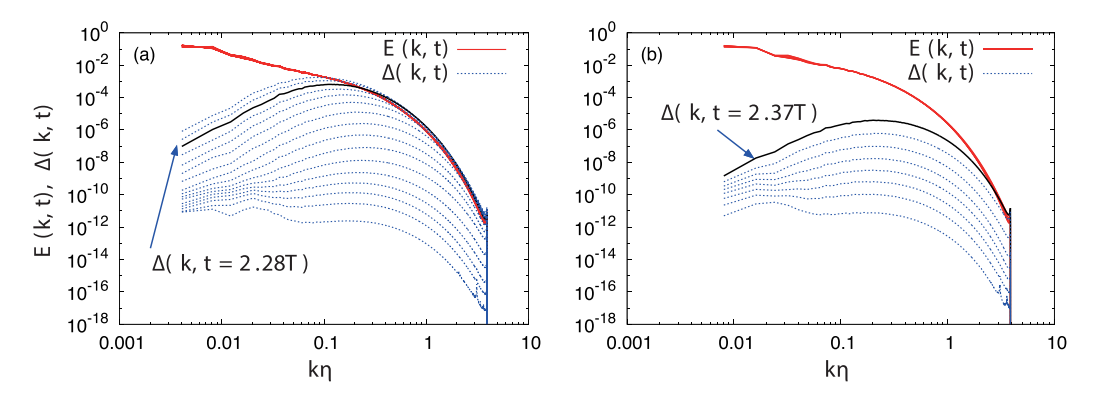


FIG. 12. Energy spectra E(k,t) and difference spectra $\Delta(k,t)$ in (a) RunH-C2 and (b) RunL-C2. The spectrum is presented in every $2000\Delta t$, which corresponds to 0.163T in the left panel and 0.296T in the right panel, respectively. For comparison, the curves of $\Delta(k,t)$ at similar time instants are shown in thick-black lines.

In this regard, recall that as mentioned in Sec. I, $\gamma(k)$ defined by (D-ii) near $k=k_{\rm max}$ can be very small, e.g., the span of $|\hat{u}(k)| (\sim k/\gamma^{1/2})$ can be larger than 10^8 or so, in the present days large-scale DNS. Although it would be too expensive to study the possible effects of the round-off error accumulation on high wave-number modes in large-scale DNS, a one-dimensional model based on a simplification of the convection term gives some quantitative idea on the effects of round-off errors that are small at each time step. See Supplemental Material for the detail [22]. In contrast to DNS of turbulent flows obeying the NS equation, the model can be easily integrated numerically for a long time. The model shows that DP or precision higher than SP is required when the magnitudes of the modes in the model span over eight orders, in agreement with the conjecture by the naive consideration noted above.

For providing a guideline on "When DP is needed," one needs to take into account that the required precision depends not only on the desired accuracy of the quantities of interest but also on factors such as the grid number N, the ratio γ , and the simulation time T_s/T , which have been discussed in detail in (D-i), (D-ii), and (D-iii) of the Introduction. Unfortunately, our current understanding seems too limited to provide more specific guidelines than those based on the naive considerations mentioned earlier and the present study, which is restricted to $R_{\lambda} \approx 268$, $N \approx 2000$, and $T_s/T \approx 2.6$.

In this respect, it would be interesting to study the influence of finite AP on the statistics of high Reynolds number turbulence in DNS of turbulent flows obeying the NS equations at higher Re, larger N, and longer T_s .

ACKNOWLEDGMENTS

This study used the computational resources of the supercomputer Fugaku provided by the RIKEN Center for Computational Science through the HPCI System Research Projects (Project IDs: hp230143 and hp240165). It was also supported by the Japan High Performance Computing and Networking plus Large-scale Data Analyzing and Information Systems (Project IDs: jh240062 and jh250074). This research was supported by the Japan Society for the Promotion of Science (KAKENHI Grants No. JP23H04473, No. JP23K11124, No. JP23K03245, and No. JP24K14986). We thank Mr. Ryotaro Ago at Okayama University for performing the computations described in the supplemental material. The authors also thank Dr. Koji Morishiata for providing the double-precision DNS code that he parallelized using the MPI library and openMP. Finally, we appreciate the valuable comments from the anonymous referees.

APPENDIX: CFL-NUMBER DEPENDENCE

In this Appendix, we examine the influence of the CFL condition on the effects of AP on DNS. The effects of the CFL number on the turbulence statistics were studied by Yeung *et al.* [4] and the effects of round-off errors were also discussed. However, their numerical schemes (second-order Runge-Kutta method, Rogallo's method to reduce aliasing errors) are different from ours, and their DNS durations are relatively short, say $10\tau_{\eta}$. Therefore, we here check the CFL dependence in our DNS.

We use here, as in Sec. III, a fourth-order Runge-Kutta method for the time marching.

Figure 13(a) compares the ratios $\epsilon_{\text{max}}/\langle\epsilon\rangle_{t=0}$ for RunH-C2 (C=0.275) and RunH-C1 (C=0.55) using DNS_{DP}. Figure 13(b) presents a similar comparison for DNS_{SP}. It is observed in Fig. 13(a) that the curves for C=0.55 and C=0.275 align closely until $t\approx 2.45T$. However, as shown in Fig. 13(b), the agreement extends only up to t<1.6T. These observations suggest that the duration over which the spatial maximum values remain unaffected by C varies depending on the AP.

In Ref. [4], $C \lesssim 0.3$ was necessary to obtain reliable results for $10\tau_{\eta}$, which is in contrast to the present results that the results of DNS_{DP} at C = 0.55 well preserve those at C = 0.275 up to

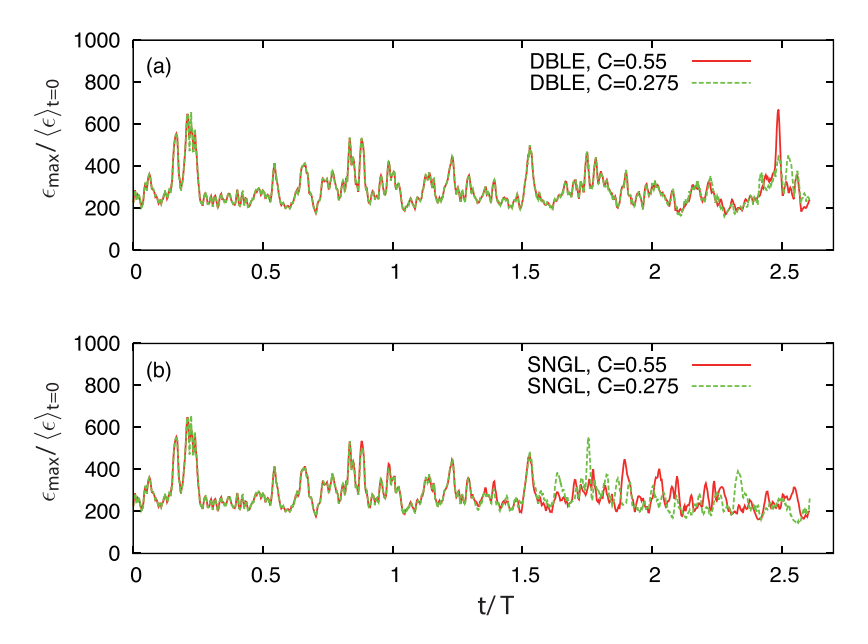


FIG. 13. (a) Comparison of $\epsilon_{\max}/\langle\epsilon\rangle_{t=0}'$ s vs t/T in RunH-C1(C=0.275) and RunH-C1(C=0.55) by DNS_{DP}. (b) The same as panel (a) but by DNS_{SP}.

 $t \approx 2.5T \approx 81.25\tau_{\eta}$. It is speculated that this is due to the difference between their work and ours in terms of the schemes and Reynolds number values.

To systematically explore this behavior, we plot $\langle \epsilon^p(\mathbf{x}, t) \rangle^{\frac{1}{p}} / \langle \epsilon \rangle_{t=0}$ using DNS_{DP} and DNS_{SP}, as shown in Fig. 14. Figure 14(a) indicates that for lower orders (p < 4), the curves for C = 0.55 and C = 0.275 by DNS_{DP} align well throughout the entire time range examined (t < 2.6T). However, for higher values of p (4 < p), the difference between the two curves becomes larger with increasing

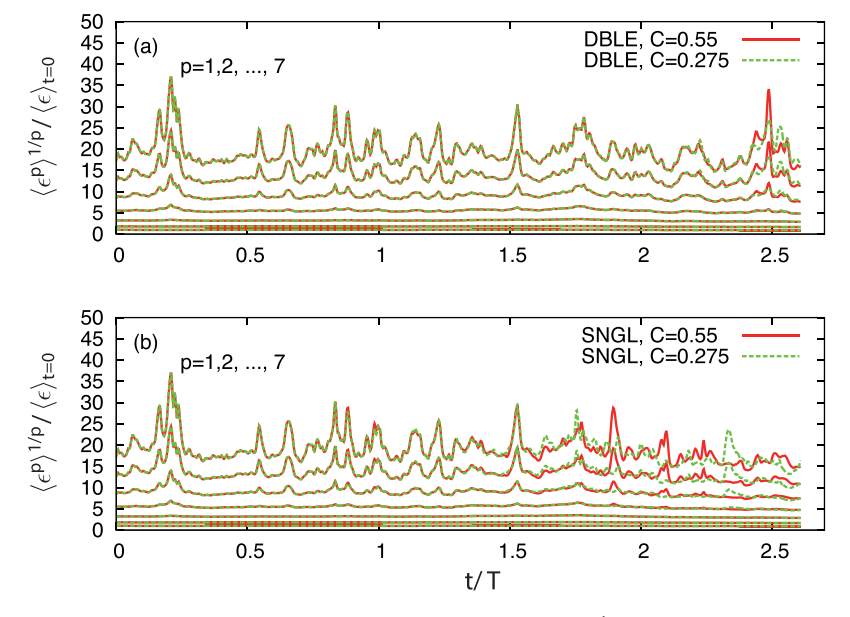


FIG. 14. Similar to Fig. 13, but for $\langle \epsilon^p(\mathbf{x}, t) \rangle^{\frac{1}{p}} / \langle \epsilon \rangle_{t=0}$.

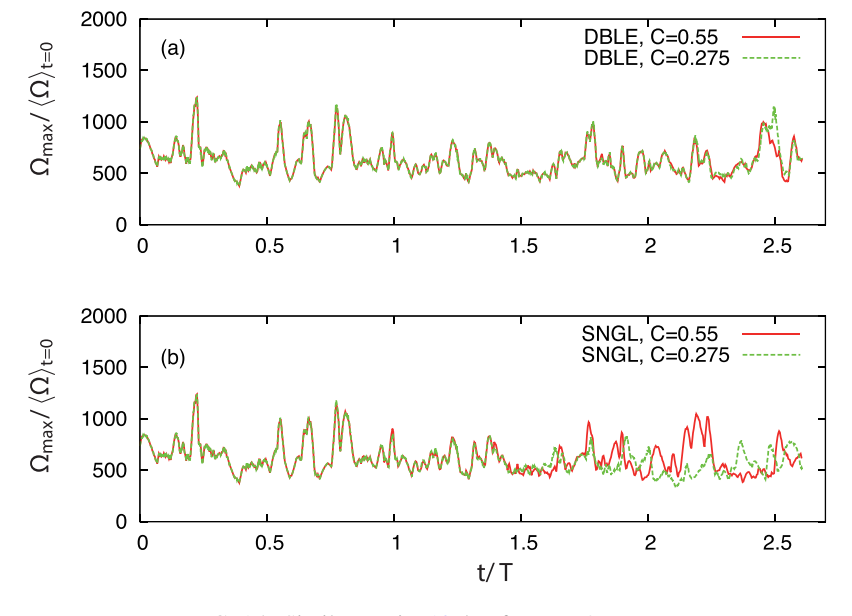


FIG. 15. Similar to Fig. 13, but for $\Omega_{\text{max}}/\langle\Omega\rangle_{t=0}$.

p after t = 2.45T. Figure 14(b) demonstrates that for lower-order statistics (p < 4) obtained by DNS_{SP}, the curves for C = 0.55 and C = 0.275 align well throughout the entire time range, similar to the observations in Fig. 14(a). In contrast, the agreement for higher-order statistics (4 < p) deteriorates after t = 1.6T.

Figures 15 and 16 show similar statistics for local enstrophy, showing that the influence of C on the effects of AP on enstrophy statistics mirrors that on the statistics of ϵ .

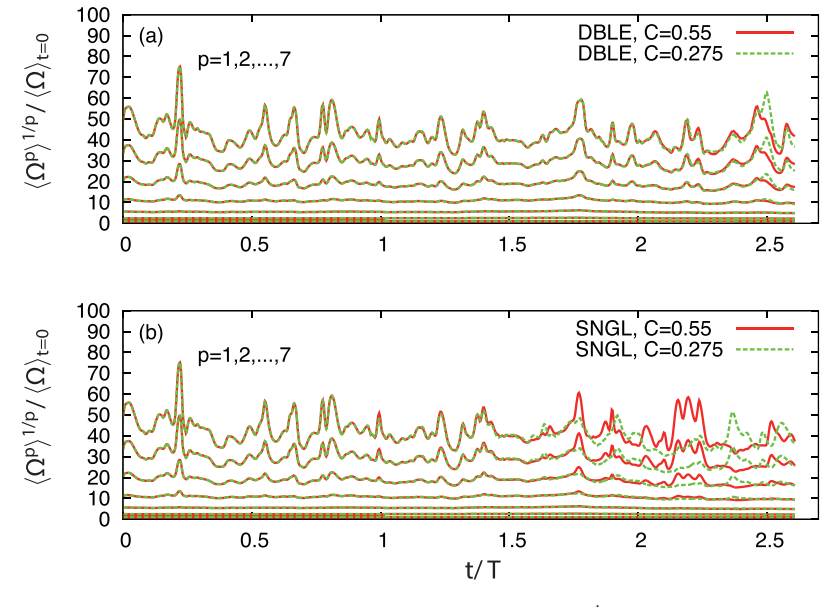


FIG. 16. Similar to Fig. 14, but for $\langle \Omega^p(\mathbf{x},t) \rangle^{\frac{1}{p}}/\langle \Omega \rangle_{t=0}$.

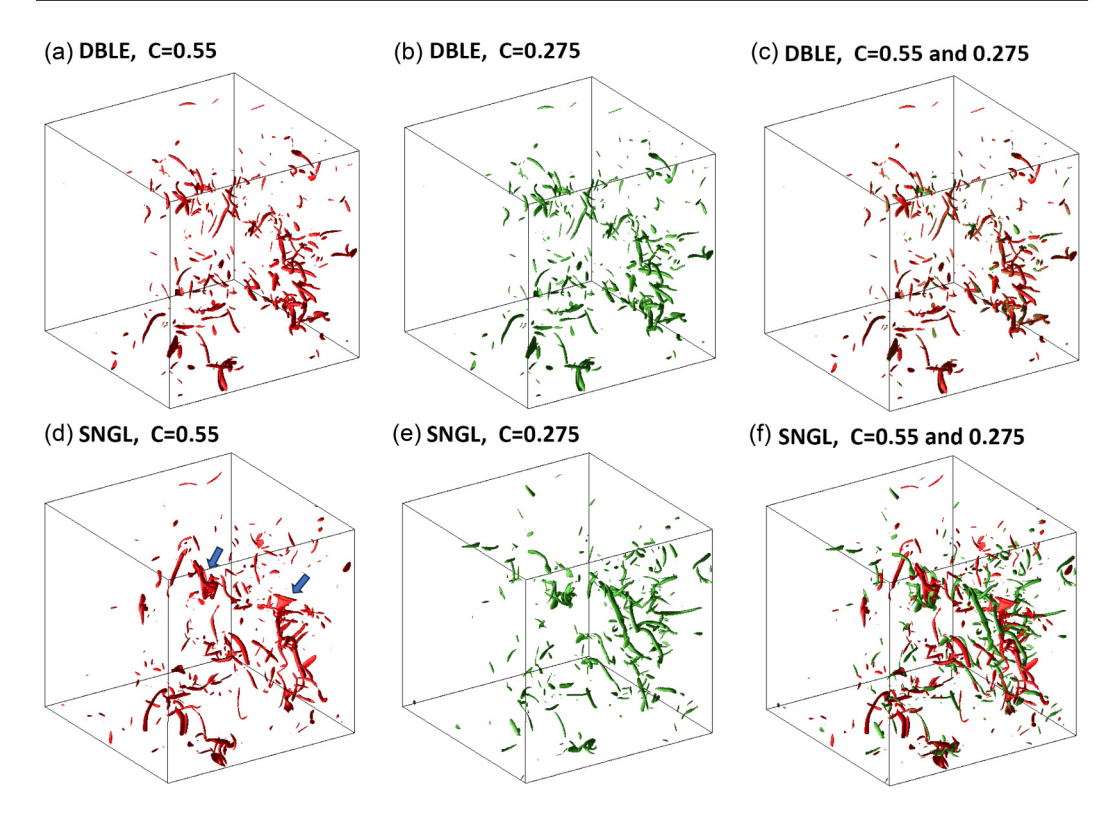


FIG. 17. Intense vorticity regions of the flow field by DNS_{DP} of (a) RunH-C1, (b) RunH-C2 at t/T=2.45, and (c) superposition of panels (a) and (b). Panels (d), (e), and (f) are the same as panels (a), (b), and (c), respectively, but by DNS_{SP}. Isosurfaces of vorticity are shown for $|\omega|=M_{\rm DP}+6.5\sigma_{\rm DP}$, where $M_{\rm DP}$ and $\sigma_{\rm DP}$ denote the mean value and standard deviation of the modulus of the vorticity field DNS_{DP} of RunH-C2.

Figure 17 illustrates intense vorticity regions at t = 2.45T for RunH-C2 and RunH-C1. In DNS_{DP}, tubelike structures are observed at both C = 0.55 and C = 0.275, with consistent positioning. Conversely, in DNS_{SP}, tubelike structures are observed for both C = 0.55 and C = 0.275, but sheetlike structures appear at C = 0.55, as indicated by arrows. This suggests that artificial structures due to insufficient AP may emerge in DNS_{SP}, depending on the C value and the visualization threshold.

^[1] A. N. Kolmogorov, The local structure of turbulence in incompressible viscous fluid for very large Reynolds number, C. R. Acad. Sci. URSS **30**, 301 (1941).

^[2] P. K. Yeung, K. Ravikumar, R. Uma-Vaideswaran, C. Meneveau, K. R. Sreenivasan, and S. Nichols, Turbulence simulations at grid resolutions of up to 32 768³ enabled by Exascale computing, in 76th Annual Meeting of the Division of Fluid Dynamics, Washington DC, No. T02.00005 (2023).

^[3] P. K. Yeung, K. Ravikumar, S. Nichols, and R. Uma-Vaideswaran, GPU-enabled extreme-scale turbulence simulations: Fourier pseudo-spectral algorithms at the exascale using OpenMP offloading, Comput. Phys. Commun. 306, 109364 (2025).

^[4] P. K. Yeung, K. R. Sreenivasan, and S. B. Pope, Effects of finite spatial and temporal resolutions on the direct numerical simulations of incompressible isotropic turbulence, Phys. Rev. Fluids 3, 064603 (2018).

- [5] H. Homann, J. Dreher, and R. Grauer, Impact of floating-point precision and interpolation scheme on the results of DNS of turbulence using pseudo-spectral codes, Comput. Phys. Commun. 177, 560 (2007).
- [6] L. P. Wang and B. Rosa, The spurious evolution of the turbulence originates from the round-off error in the pseudo-spectral simulation, Comput. Fluids 38, 1943 (2009).
- [7] D. A. Donzis, P. K. Yeung, and K. R. Sreenivasan, Dissipation and enstrophy in isotropic turbulence: Resolution effects and scaling in direct numerical simulations, Phys. Fluids **20**, 045108 (2008).
- [8] P. K. Yeung, X. M. Zhai, and K. R. Sreenivasan, Extreme events in computational turbulence, Proc. Natl. Acad. Sci. USA 112, 12633 (2015).
- [9] D. Buaria, A. Pumir, E. Bodenschatz, and P. K. Yeung, Extreme velocity gradients in turbulent flows, New J. Phys. 21, 043004 (2019).
- [10] D. Buaria, A. Pumir, and E. Bodenschatz, Self-attenuation of extreme events in Navier-Stokes turbulence, Nat. Commun. 11, 5852 (2020).
- [11] D. Buaria, E. Bodenschatz, and A. Pumir, Vortex stretching and enstrophy production in high Reynoldsnumber turbulence, Phys. Rev. Fluids 5, 104602 (2020).
- [12] T. Gotoh, T. Watanabe, and I. Saito, Kinematic effects on probability density functions of energy dissipation rate and Enstrophy in turbulence, Phys. Rev. Lett. **130**, 254001 (2023).
- [13] D. Buaria and A. Pumir, Vorticity-strain rate dynamics and the smallest scales of turbulence, Phys. Rev. Lett. 128, 094501 (2022).
- [14] P. K. Yeung, D. A. Donzis, and K. R. Sreenivasan, Dissipation, enstrophy and pressure statistics in turbulence simulations at high Reynolds numbers, J. Fluid Mech. **700**, 5 (2012).
- [15] Y. Kaneda, T. Ishihara, M. Yokokawa, K. Itakura, and A. Uno, Energy dissipation rate and energy spectrum in high-resolution direct numerical simulations of turbulence in periodic box, Phys. Fluids 15, L21 (2003).
- [16] M. Yokokawa, K. Itakura, A. Uno, T. Ishihara, and Y. Kaneda, 16.4-Tflops direct numerical simulation of turbulence using a Fourier spectral method on the Earth Simulator, in *Proceedings of the ACM/IEEE Conference on Supercomputing* (IEEE, Piscataway, NJ, 2002), p. 50.
- [17] T. Ishihara, Y. Kaneda, M. Yokokawa, K. Itakura, and A. Uno, Small-scale statistics in high-resolution direct numerical simulations of turbulence: Reynolds number dependence of one-point velocity gradient statistics, J. Fluid Mech. 592, 335 (2007).
- [18] R. S. Rogallo, Numerical experiments in homogeneous turbulence, NASA Tech. Memo. 81315 (NASA Ames Research Center, 1981).
- [19] T. Ishihara, T. Gotoh, and Y. Kaneda, Study of high-Reynolds-number isotropic turbulence using direct numerical simulations, Annu. Rev. Fluid Mech. 41, 165 (2009).
- [20] Lorenz, Deterministic nonperiodic flow, J. Atmos. Sci. 20, 130 (1963).
- [21] N. Okamoto, T. Matsuzaki, M. Yokokawa, and Y. Kaneda, Effects of temporal and spatial schemes on direct numerical simulations of incompressible isotropic turbulence, HPCI Res. Rep. 8, 1 (2023).
- [22] See Supplemental Material at http://link.aps.org/supplemental/10.1103/PhysRevFluids.10.064603 for further details on the long-term computation of a model equation, providing insight into the effects of round-off errors on the DNS of high-Re turbulence, where modes with vastly different magnitudes coexist.